

Dynamics and evaporation of defects in Mott-insulating clusters of boson pairs

Dominik Muth,^{1,2,*} David Petrosyan,^{1,3} and Michael Fleischhauer¹

¹*Fachbereich Physik und Forschungszentrum OPTIMAS,*

Technische Universität Kaiserslautern, D-67663 Kaiserslautern, Germany

²*Graduate School Materials Science in Mainz, Technische Universität Kaiserslautern, D-67663 Kaiserslautern, Germany*

³*Institute of Electronic Structure and Laser, FORTH, GR-71110 Heraklion, Crete, Greece*

(Dated: June 2, 2022)

Repulsively bound pairs of particles in a lattice governed by the Bose-Hubbard model can form stable incompressible clusters of dimers corresponding to finite-size $n = 2$ Mott insulators. Here we study the dynamics of hole defects in such clusters corresponding to unpaired particles which can resonantly tunnel out of the cluster into the lattice vacuum. Due to bosonic statistics, the unpaired particles have different effective mass inside and outside the cluster, and “evaporation” of hole defects from the cluster boundaries is possible only when their quasi-momenta are within a certain transmission range. We show that quasi-thermalization of hole defects occurs in the presence of catalyzing particle defects which thereby purify the Mott insulating clusters. We study the dynamics of one-dimensional system using analytical techniques and numerically exact t-DMRG simulations. We derive an effective strong-interaction model that enables simulations of the system dynamics for much longer times. We also discuss a more general case of two bosonic species which reduces to the fermionic Hubbard model in the strong interaction limit.

PACS numbers: 37.10.Jk, 03.75.Lm, 67.80.dj, 05.30.Jp,

I. INTRODUCTION

Quantum particles in lattice potentials, e.g. electrons in crystals, have been studied since the early days of quantum theory [1, 2]. With the development of artificial (optical) lattice potentials for cold neutral atoms [3], bosonic lattice models are recently attracting increased interest as well [4], with the Bose-Hubbard model (BHM) [5] being an important example. A remarkable phenomenon entailed by the BHM is that pairs of strongly interacting bosons can form tightly bound “dimers” both for attractive and repulsive interactions [6–9]. In free space, or in the presence of energy dissipation, the repulsive interaction inevitably leads to pair dissociation. In a lattice, however, the kinetic energy of each particle is restricted to the values in the allowed Bloch band. Consequently, two co-localized particles in a dissipation-free lattice remain tightly bound together as a dimer when their interaction energy U exceeds the kinetic energy of free particles $\sim J$ within the Bloch band.

In a previous publication [9], we have studied the many-body dynamics of the repulsively-bound dimers of bosons. Due to virtual transitions of the dimer constituent particles, the dimers at the neighboring lattice sites strongly attract each other, with the corresponding interaction energy exceeding the dimer tunneling energy by a factor of 4. For many dimers on the lattice, it is then energetically favorable to form dynamically stable “droplets”, constituting incompressible Mott-insulating (MI) clusters with the number of particles per site of exactly $n = 2$. Inevitable imperfections in the preparation process would typically cause such MI clusters to contain hole and particle defects corresponding, respectively, to unpaired and excess particles (monomers and trimers). An

important question is thus how to purify the system of the defects reducing thereby the entropy. In the present paper, we discuss a mechanism of self-purification of stable MI clusters of dimers surrounded by lattice vacuum. We study the dynamics of defects in one-dimensional system by analytical calculations and numerical many-body simulations.

Within the cluster, hole and particle defects can propagate via resonant single-particle hopping with enhanced amplitude, which stems from the bosonic statistics of the surrounding $n = 2$ MI environment. Outside the cluster, hole defects correspond to free particles. Since their tunneling energy J is much larger than the monomer-dimer interaction energy $\sim J^2/U$ [10], hole defects are not bound to the cluster and can “evaporate”. However, the widths of the single particle Bloch band is twice larger inside the cluster than outside of it, therefore only the hole defects with energies in the center of the band can penetrate the cluster boundaries and evaporate into the lattice vacuum, while in the absence of quasi-momentum redistribution, low- and high-energy hole defects will remain in the cluster. We show that the presence of particle defects leads to efficient “thermalization” of the hole defects via quasi-momentum redistributing collisions. Hence, very few such “catalyzing” particle defects can purify the MI cluster.

Before continuing, we note a recent relevant work [11] dealing with fermionic dimers described by the Hubbard model. After preparing a cold atomic gas with filling of $n \simeq 2$ in the trap center, followed by turning off the trap, the hole defects will simply tunnel out of the cluster into the vacuum. For fermions, however, the remaining cluster is not stable, since the effective second-order tunneling of the on-site pairs is not restrained by the interaction between the pairs.

Figure 1 illustrates the main physics studied in this paper, which is organized as follows. In Sec. II we outline the properties of the pure dimer clusters [9]. We then introduce in Sec. III an effective theory of scattering of a single particle

*Electronic address: muth@physik.uni-kl.de

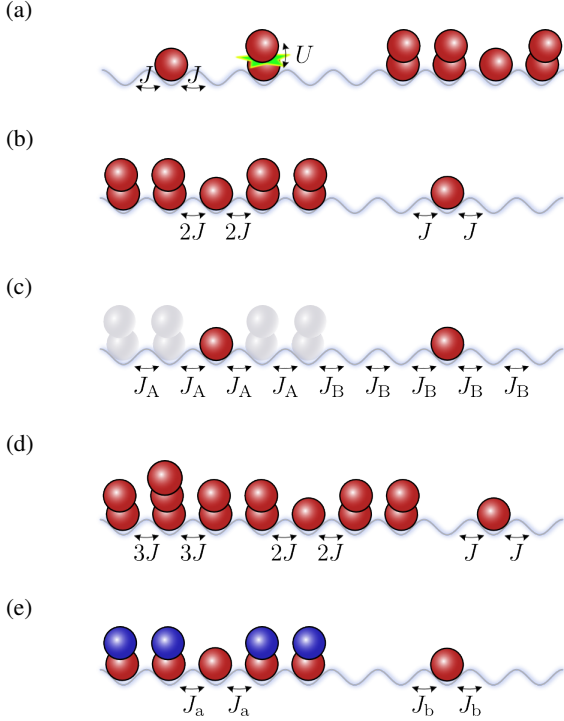


FIG. 1: (Color online) Physical models studies in this paper. (a) The Bose-Hubbard model, Eq. (1). (b) Monomer (hole defect) effective hopping, Sec. III. (c) Single defect effective theory, Sec. III. (d) Trimer (particle defect) effective hopping, Sec. IV. (e) Single hole defect in two species Bose-Hubbard model, Sec. VI.

(hole defect) from a domain wall separating the dimer cluster and the vacuum. The quasi-momentum redistribution of a hole defect upon collisions with a particle defect in the lattice with periodic and open boundaries is studied in Sec. IV. In Sec. V we present the results of many-body numerical simulations for a realistic system with several hole and particle defects in a dimer cluster surrounded by empty lattice. Finally, in Sec. VI we discuss the case of two bosonic species, which is more flexible theoretically, but is demanding experimentally. In the limit of infinite intra-species interaction, it contains the special case of the Hubbard model [11], since in one dimension and in the absence of double occupancy, bosons and fermions are equivalent through the Jordan-Wigner transformation. Much of the involved technical details are deferred to Appendices A, B, C and D.

II. REPULSIVELY BOUND DIMERS

The underlying Hamiltonian for our system is that of the BHM [5]

$$\hat{H} = -J \sum_j (\hat{b}_j^\dagger \hat{b}_{j+1} + \text{H.a.}) + \frac{1}{2} U \sum_j \hat{b}_j^\dagger \hat{b}_j^\dagger \hat{b}_j \hat{b}_j, \quad (1)$$

where \hat{b} and \hat{b}^\dagger are bosonic annihilation and creation operators, J is the particle hopping rate between adjacent lattice sites $j, j+1$, and U is the contact interaction between the

particles on the same lattice site. Throughout this paper, we assume that the on-site interaction is the dominant energy parameter, $U \gg J$.

Considering first a lattice containing only zero or two particles per site, we do not allow the dimer occupation number in the lattice to exceed unity. Adiabatically eliminating all the states with odd number of particles per site, we obtain for the dimers an effective Hamiltonian [9] that contains only terms with characteristic energies on the scale of $J^2/U \ll J$:

$$\hat{H} = -\tilde{J} \sum_j (\hat{c}_j^\dagger \hat{c}_{j+1} + \text{H.a.}) + \tilde{B} \sum_j \hat{c}_j^\dagger \hat{c}_{j+1}^\dagger \hat{c}_{j+1} \hat{c}_j, \quad (2)$$

where $\tilde{J} = -2J^2/U$ is the dimer hopping rate and $\tilde{B} = -16J^2/U$ is the nearest neighbor interaction. The dimer creation \hat{c}_j^\dagger and annihilation \hat{c}_j operators satisfy the hard-core boson commutation relations

$$i \neq j: \quad [\hat{c}_i, \hat{c}_j] = [\hat{c}_i, \hat{c}_j^\dagger] = 0, \quad (3a)$$

$$i = j: \quad \{\hat{c}_j, \hat{c}_j\} = 0, \{\hat{c}_j, \hat{c}_j^\dagger\} = 1. \quad (3b)$$

Hamiltonian (2) can be mapped onto that for the spin- $\frac{1}{2}$ XXZ model [12, 13] with the anisotropy parameter $\Delta = \tilde{B}/2\tilde{J} = 4$. For $\Delta > 1$, we are in the ferromagnetic, Ising-like regime, and a cluster of dimers, corresponding to a lattice domain with maximum magnetization, is dynamically stable. To understand this in terms of dimers, observe that, for any $U(\gg J)$, the maximal kinetic energy $2\tilde{J}$ gained by releasing a dimer from the cluster boundary is small compared to the binding energy \tilde{B} of the dimer to the cluster.

The stability of the dimer cluster is an intrinsic feature of the BHM. It is rooted in the bosonic amplification of the inter-site hopping of the particles, which in turn enhances the effective (second-order) nearest neighbor interaction \tilde{B} . For the fermionic Hubbard model discussed in [11] in the context of defect evaporation from a dimer cluster, i.e., a band insulator, we show in Sec. VI that $\Delta = 1$ ($\tilde{B} = 2\tilde{J}$), which means that the cluster is unstable and the dimers will diffuse away.

III. SINGLE DEFECT MODEL IN THE STRONG-INTERACTION LIMIT

The dynamics of dimers is rather slow, as it is governed by the small characteristic energies $\sim J^2/U$, but the dynamics of monomers is much faster, involving large single-particle hopping rate J . We can thus retain only the contributions on the scale of J , which results in a very simple and transparent effective theory for the monomers. For a monomer in the cluster (hole defect), the bosonic statistics plays an important role: it increases the hopping amplitude of the monomer in the environment of dimers by a factor of 2, see Fig. 1(b). As a result, the kinetic energy of the monomer in the dimer cluster is $E_k = -4J \cos(k)$, while in the vacuum it is $E_k = -2J \cos(k)$, where $k \in [-\pi, \pi]$ is the monomer quasi-momentum quantified by the phase change between neighboring lattice sites. Therefore the monomer will be confined to

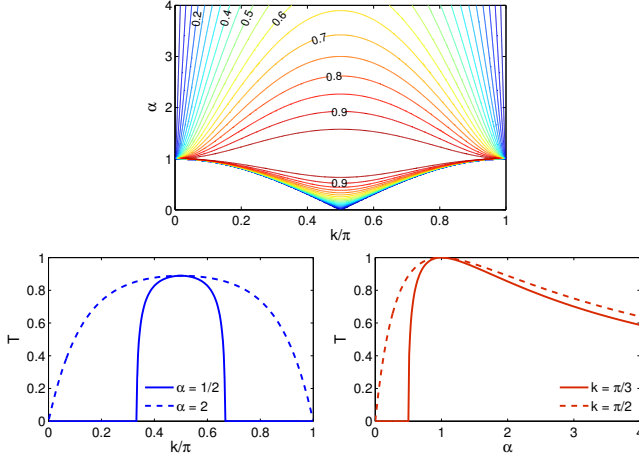


FIG. 2: (Color online) Transmission probability $T(k)$ [cf. Eq. (A9)] for various $\alpha = J_B/J_A$.

the cluster if its quasi-momentum is not inside the transmission region given by

$$k \in (-2\pi/3, -\pi/3) \cup (\pi/3, 2\pi/3), \quad (4)$$

up to a correction due to small interactions of the order of $J^2/U \ll J$ which we neglected.

Consider the scattering of a monomer from the domain wall between the dimer cluster occupying sites $j < 0$ (region A) and the vacuum at sites $j > 0$ (region B), see Fig. 1(c). The local bare particle number is $n_j = 2$ for $j < 0$ and $n_j = 0$ for $j > 0$. The particle number at $j = 0$ depends on the position i of the monomer $n_i = 1$: inside the cluster $i < 0$ we have $n_0 = 2$, at the boundary $i = 0$ obviously $n_0 = 1$, while outside the cluster (in the vacuum) $i > 0$ leads to $n_0 = 0$. Hence the position of the wall shifts upon the monomer crossing the boundary, which should be taken into account when considering many defects. The hopping rate of the monomer is J_A for sites $j \leq 0$ and J_B for sites $j > 0$. The effective Hamiltonian for a single monomer then reads

$$\hat{H} = -J_A \sum_{j<0} (\hat{a}_j^\dagger \hat{a}_{j+1} + \text{H.a.}) - J_B \sum_{j \geq 0} (\hat{a}_j^\dagger \hat{a}_{j+1} + \text{H.a.}), \quad (5)$$

with $J_A = 2J$ and $J_B = J$.

In Appendix A we calculate the exact transmission probability $T(k)$ of a particle crossing a domain wall in a system described by Hamiltonian (5). The results are illustrated in Fig. 2 for various $\alpha = J_B/J_A$. The values of $\alpha = 1/2$ and $\alpha = 2$ correspond, respectively, to the single particle leaving the dimer cluster and entering it from vacuum.

IV. QUASI-MOMENTUM REDISTRIBUTION OF THE DEFECTS

We have seen above that a hole defect can leave the MI cluster only if its quasi-momentum is within the transmission range of Eq. (4), while a defect with the quasi-momentum

outside the transmission range will remain in the cluster indefinitely. Hence, to completely purify the cluster of hole defects, their quasi-momenta should be continuously redistributed over the entire range of $k \in [-\pi, \pi]$. In two or more dimensions, collisions between identical particles can redistribute the absolute values of their quasi-momenta, and we therefore expect the evaporation of all the defects through the cluster boundaries after a few collisions. In a one dimensional lattice, however, collisions of two particles interacting via any finite range potential can only exchange their quasi-momenta or leave the quasi-momenta unchanged [7, 8, 14, 15] (for indistinguishable particles both outcomes are equivalent), provided that the lattice is deep enough so that the large band gap precludes interband transitions. Similarly, collisions with the fixed boundaries can only reverse the quasi-momentum of a particle. The simplest quasi-momentum redistribution mechanism is then three particle collisions. This happens at a rate proportional to the defect density squared, which is too slow for cold atom experiments.

In the dimer cluster, in addition to the hole defects (monomers), we may have particle defects (trimers) with different effective mass. The hopping rates of a monomer and a trimer in the cluster are $J_a = 2J$ and $J_t = 3J$, respectively, Fig. 1(d). Before collision, their quasi-momenta are k_a and k_t , while conservations of quasi-momentum, $k_a + k_t = k'_a + k'_t$, and energy, $J_a \cos(k_a) + J_t \cos(k_t) = J_a \cos(k'_a) + J_t \cos(k'_t)$, during the collision determine the new quasi-momenta k'_a and k'_t via

$$J_a \cos(k_a) + J_t \cos(k_t) = J_a \cos(k'_a) + J_t \cos(k_a + k_t - k'_a). \quad (6)$$

If there is a collision with the wall, or a third defect of either kind, before this process is reversed, all energetically allowed combinations of k_a, k_t can be assumed, as will be verified below by exact numerical simulations.

A. Two classical particles

The timescale for quasi-momentum redistribution can be calculated from purely classical considerations. A monomer or a trimer moving in the MI cluster has a kinetic energy of $E_{k_\mu} = -2J_\mu \cos(k_\mu)$ and the corresponding group velocity of $v_\mu = 2J_\mu \sin(k_\mu)$ [$\mu = a, t$].

Consider first two wave packets in a periodic lattice of length L . After a collision (the defects can not penetrate each other), their velocities are assumed to be $v_a = 2J_a \sin(k_a) < v_t = 2J_t \sin(k_t)$. The next collision happens after time

$$t_c = \frac{L-1}{2} \frac{1}{J_t \sin(k_t) - J_a \sin(k_a)}, \quad (7)$$

and the new quasi-momenta are determined by Eq. (6). It follows that the time interval between all subsequent collisions is the same $t_c/2$, since Eq. (6) and

$$\begin{aligned} & \frac{L-1}{2} \frac{1}{J_t \sin(k_t) - J_a \sin(k_a)} \\ &= \frac{L-1}{2} \frac{1}{-J_t \sin(k_a + k_t - k'_a) + J_a \sin(k'_a)} \end{aligned}$$

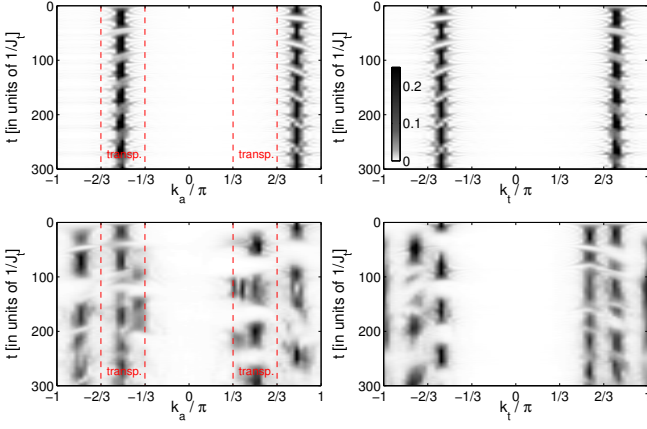


FIG. 3: (Color online) Dynamics of the quasi-momentum distribution for the monomer (left column) and trimer (right column) in a lattice of $L = 64$ sites. The initial quasi-momenta are $k_a = \frac{13}{16}\pi$ and $k_t = -\frac{9}{16}\pi$. Upper panels correspond to periodic boundary conditions, where the markers on the right indicate multiples of the revival time $t_c \approx 46.63/J_t$. Lower Panels are obtained for open boundary conditions. Dashed vertical lines mark the transmission regions for monomer quasi-momenta as per Eq. (4).

always have a common solution.

In the presence of a wall, or a third defect, the quasi-momenta can take any values energetically allowed. A revival is not expected, but now t_c^{-1} is an effective rate of quasi-momentum redistribution. It is essentially given by J over the mean free path, i.e., it is proportional to J times the average defect density, which is indeed much faster than the rate of three particle collisions.

B. Two quantum particles: Numerical simulations

We simulate the quantum dynamics of the hole and particle defects in a dimer cluster using the two-particle Hamiltonian in quasi-momentum space, see Appendix B. Each defect is initially prepared in a quasi-momentum eigenstate, with the combined state given by

$$|k_a, k_t\rangle = \frac{1}{L} \sum_{j_a, j_t=1}^L e^{ik_a j_a} e^{ik_t j_t} \hat{a}_{j_a}^\dagger \hat{t}_{j_t}^\dagger |\text{vac}\rangle, \quad (8)$$

where \hat{a}_j^\dagger creates a monomer and \hat{t}_j^\dagger a trimer at site j of a finite lattice filled with dimers, playing here the role of an effective vacuum $|\text{vac}\rangle$.

Figure 3 shows the results of our numerical simulations. In the case of periodic boundary conditions, the dynamics is mainly classical; only two values of quasi-momentum k are assumed by each particle, and after the classical revival time t_c , the quasi-momentum distribution is restored to the initial. For open boundary conditions, however, we observe fast redistribution of quasi-momenta, and already the first revival is hardly noticeable. We may therefore conclude that a single trimer can catalyze the redistribution of quasi-momenta of

monomers, making the evaporation of almost all hole defects possible, provided that their average kinetic energy is initially close to the center of the band. This will be verified by the following many-body calculations.

V. MANY-BODY NUMERICAL SIMULATIONS

To study the dynamics of several defects under experimentally realistic conditions, we use a sufficiently long lattice that can accommodate dimer clusters spanning a few dozen sites. The complete Hilbert space for such a system is too large to be amenable to exact diagonalization treatments. We therefore resort to time-dependent density matrix renormalization group (t-DMRG) methods [16, 17], specifically, the time evolving block decimation (TEBD) algorithm [18] using the matrix product state (MPS) formalism. Even then, however, simulating the full BHM is a difficult task. This is due to sizable quantum fluctuations present even in the pure dimer cluster for any finite interaction strengths U/J . These fluctuations contribute to the many-body entanglement and consume much of the computational resources required to simulate the dynamics of the defects. We therefore introduce an effective model for the defects only.

A. Many defect effective theory in the strong-interaction limit

Since the states with different number of particles per site have energies separated by multiples of $U (\gg J)$, the numbers of monomers, dimers, and trimers in a lattice are, to a good approximation, conserved separately. This allows us to treat the monomers, dimers, and trimers as distinguishable species, each represented by hard-core bosons, Eqs. (3). Furthermore, as discussed in Sec. II, dimers forming stable clusters do not contribute to the dynamics of the system. For our initial conditions, typically containing a single cluster, we can thus reformulate the problem as one of the hole and particle defects moving on the background of dimers or vacuum, with the spatial configuration of the dimer cluster entering the effective Hamiltonian for the defects only as a parameter.

We define the reference system in which the pure dimer cluster occupies certain lattice sites while all the defects are placed at the beginning (left side) of the lattice. As the defects move in the lattice, the effective hopping rates depend on whether they are inside or outside the MI cluster. In turn, the position of the cluster depends on the positions of the defects, since each defect crossing the system from the left to the right shifts the position of the dimers, and the cluster as a whole, by one site to the left. The effective Hamiltonian for the defects can then be cast as

$$\hat{H} = \sum_{j=1}^{L-1} \sum_{n_r=0}^N \hat{H}_j^{[\Theta(j+n_r)]} \otimes \hat{P}_{[j+2, L]}^{n_r} \equiv \sum_{j=1}^{L-1} \tilde{H}_j, \quad (9)$$

where $\hat{P}_{[j+2, L]}^{n_r}$ is the projector onto the subspace containing exactly n_r hole and particle defects on sites $j+2$ to L , while

each local operator $\hat{H}_j^{[\Theta]}$ acts on sites j and $j + 1$ as

$$\begin{aligned} \hat{H}_j^{[\Theta]} = & -J_a^{[\Theta]}(\hat{a}_j^\dagger \hat{a}_{j+1} + \text{H.a.}) \hat{t}_j \hat{t}_{j+1} \hat{t}_{j+1}^\dagger \hat{t}_j^\dagger \\ & -J_t^{[\Theta]}(\hat{t}_j^\dagger \hat{t}_{j+1} + \text{H.a.}) \hat{a}_j \hat{a}_{j+1} \hat{a}_{j+1}^\dagger \hat{a}_j^\dagger. \end{aligned} \quad (10)$$

Here \hat{a}_j^\dagger and \hat{a}_j (\hat{t}_j^\dagger and \hat{t}_j) are the hard-core bosonic creation and annihilation operators for the monomers (trimers). The function $\Theta(j)$ is initialized for all j with respect to the reference system, and it can take two values: $\Theta(j) = 1$ for site $j + 1$ being empty (vacuum) and $\Theta(j) = 2$ for site $j + 1$ containing a dimer. Then the hopping rates for the monomers are $J_a^{[1]} = J$ and $J_a^{[2]} = 2J$, and for the trimers are $J_t^{[1]} = 0$ (they can not move on an empty lattice in first order in J) and $J_t^{[2]} = 3J$.

Note that since the effective Hamiltonian (10) contains two species of particles with hardcore interactions, it can not be mapped onto a model of free fermions via the Jordan-Wigner transformation (which is possible for identical hard-core bosons). The dynamics is therefore non-trivial and actual calculations again require numerical many-body (TEBD) techniques. The practical advantage of the effective model—besides the largely reduced number of particles—is that the fast timescale U^{-1} is eliminated from the system's dynamics and in our numerical simulations we can choose Trotter steps on the time scale $\lesssim J^{-1}$. Further discussion on the effective defect model is given in Appendix C.

B. Initial states

In our numerical calculations, we use several typical configurations of the defects in the lattice, each configuration described by a pure quantum state. Various coherent and incoherent superpositions of such configurations would represent mixed initial states.

We consider piecewise product states. A MI segment of length l contains fixed number of particles n at every site ($n = 2$ inside the dimer cluster and $n = 0$ in the vacuum),

$$|\cdot\rangle_l^n = \bigotimes_{j=1}^l \frac{(\hat{a}_j^\dagger)^n}{\sqrt{n!}} |\text{vac}\rangle, \quad (11)$$

with $|\text{vac}\rangle$ denoting the true vacuum. Each segment can contain an additional defect. For a defect localized as site j , we use the notation

$$|j+\rangle_l^n = \frac{\hat{a}_j^\dagger}{\sqrt{n+1}} |\cdot\rangle_l^n, \quad (12a)$$

$$|j-\rangle_l^n = \frac{\hat{a}_j}{\sqrt{n}} |\cdot\rangle_l^n \quad (n \geq 1), \quad (12b)$$

with \pm corresponding, respectively, to a particle and a hole defect. Similarly, we denote a defect with quasi-momentum

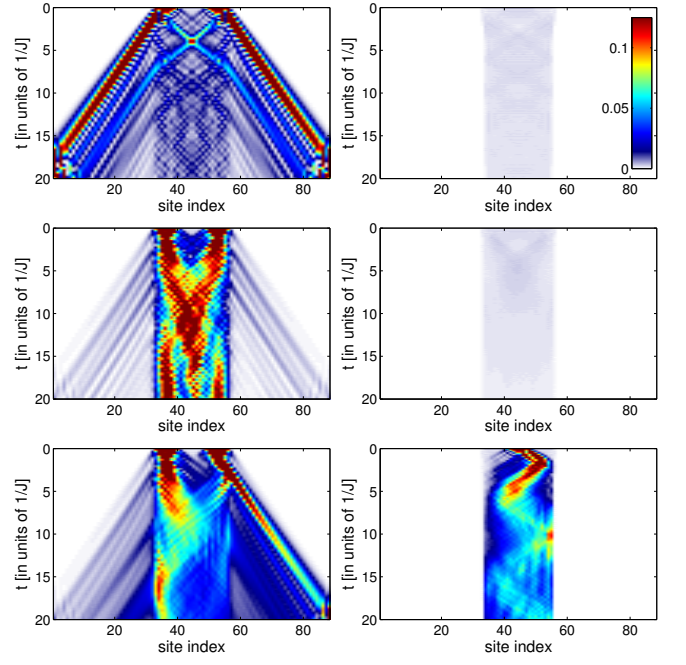


FIG. 4: (Color online) Density of monomers (left column) and trimers (right column) in the $n = 2$ MI cluster of 24 sites surrounded by empty lattice, $|\cdot\rangle_{32}^0$, on both sides. In the top panels, the initial state of the cluster $|\pi/2\rangle_8^2 |\pi/2\rangle_8^2$ corresponds to two monomers at the center of the band moving to the left and right. In the central panel, the initial state $|\pi\rangle_8^2 |\pi\rangle_8^2$ corresponds to two monomers at the upper and lower band edges. In the bottom panel, the initial state $|\pi\rangle_8^2 |\pi/2\rangle_8^2 |0\rangle_8^2$ is the same as in the central panels plus a particle defect at the center of the band, moving to the right. The interaction strength is $U = 100J$. The density of monomers (trimers) corresponds to the probability of finding exactly one (three) particles at a given site. A TEBD [18] algorithm with bond dimension $\chi = 200$ is used for the time evolution with a fourth order Trotter decomposition and time step size $1/50J$, with particle number conservation explicitly included in the MPS [19].

k , which must be a multiple of $2\pi/l$, as

$$|k\rangle_l^{n+} = \frac{1}{\sqrt{l}} \sum_{j=1}^l e^{ikj} |j+\rangle_l^n, \quad (13a)$$

$$|k\rangle_l^{n-} = \frac{1}{\sqrt{l}} \sum_{j=1}^l e^{ikj} |j-\rangle_l^n \quad (n \geq 1). \quad (13b)$$

We prepare the cluster by joining MI segments with and without defects. Since we are only interested in low defect densities, we do not construct segments containing multiple defects. In order to perform TEBD simulations, the initial states have to be represented in the MPS form, which is discussed in Appendix D.

C. Numerical results

Figures 4 and 5 show the time evolution of defects in a $n = 2$ MI cluster surrounded by vacuum, obtained from the

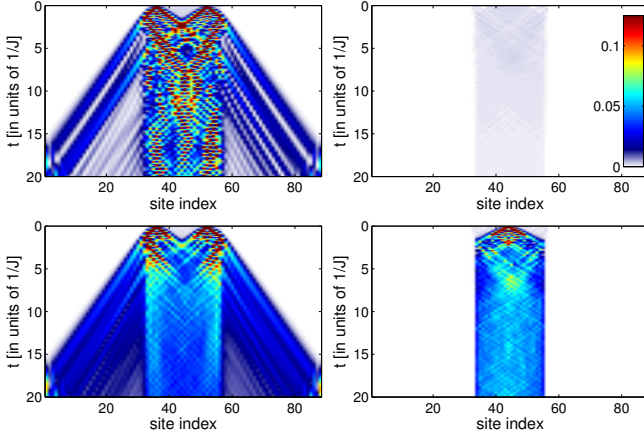


FIG. 5: (Color online) Same as Fig. 4 but for localized initial states: Top panel, $|4_-\rangle_8^2 | \cdot \rangle_8^2 |4_-\rangle_8^2$, two localized monomers; bottom panel, $|4_-\rangle_8^2 |4_+\rangle_8^2 |4_-\rangle_8^2$, same plus a localized trimer.

full BHM. Hole defects with quasi-momenta at the center of the band can easily leave the cluster after just a few scattering events, Fig. 4. Hole defects prepared at the edges of the band remain trapped in the cluster. An additional particle defect, which itself can not leave the cluster, induces fast quasi-momentum redistribution of the hole defects, large fraction of which can now leave the cluster.

The same effect is observed with localized defects, Fig. 5. For hole defects alone, about one third of their population leaves the cluster (note that the localized initial state of each defect has uniform distribution of quasi-momentum $k \in [-\pi, \pi]$, and not energy $E_k \in [-4J, 4J]$), while an additional localized particle defect increases this fraction significantly.

In Fig. 6(a) and (b) we show the time evolution of the total population of monomers outside the dimer cluster pertaining to the cases illustrated in Figs. 4 and 5, respectively. Again, hole defects with quasi-momenta in the center of the band easily escape the cluster even without the assistance of a particle defect, Fig. 6(a). Conversely, for the hole defects with quasi-momenta at the edges of the Bloch band in the cluster, very little population is found outside the cluster in the long time limit (the small fraction of monomer population in the vacuum is due to the finite binding energy U of the dimers). Adding a particle defect in the cluster significantly increases the fraction of monomers outside the cluster; we find that the increase is always larger for a particle defect in the center of the band than for a localized one.

For the initially localized hole defects, Fig. 6(b), and without assistance of a particle defect, we find that, as expected, about a third of their total population occupying the center of the Bloch band leaves the cluster in the long-time limit. A particle defect can further increase the portion of escaping population of the hole defects by redistributing their quasi-momenta over the entire band.

Note that the results of numerical simulations for the system with a particle defect are reliable for shorter times as compared to the simulations with the hole defects only, which is

due to the larger entanglement created dynamically upon the trimer-monomer collisions.

So far we have been restricted to the treatment of only two monomers and one trimer and for relatively short times, because in the full BHM the fast growing entanglement in the system limits the numerical method. With the effective model containing only the hole and particles defects, we can simulate the dynamics for much longer times with the same numerical accuracy, as can be seen in Fig. 6. The perfect agreement between the full and effective models allows us to employ the effective model for simulating larger systems and for longer times.

Fig. 7 shows numerical results for a system containing initially up to four defects. As expected, the evaporation works for the larger systems as well. Most importantly, in the presence of a particle defects, the number of hole defects left in the cluster in the long-time limit falls well below unity (extrapolating the curves to somewhat larger times than shown in Fig. 7, if necessary).

VI. TWO SPECIES BOSE-HUBBARD MODEL

We have seen in the previous sections that, in the single species BHM, the hopping amplitudes of a monomer inside an $n = 2$ MI cluster and on an empty lattice differ by a fixed factor of 2. More flexibility is offered by the two species BHM,

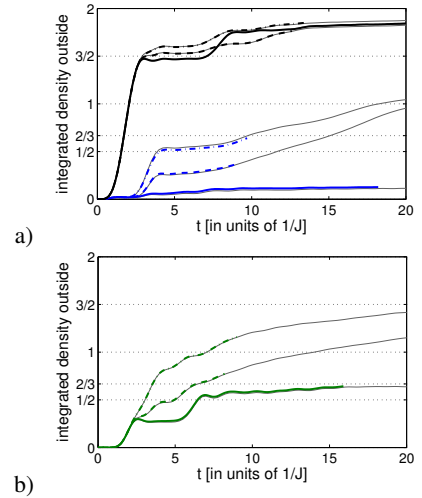


FIG. 6: (Color online) Total population (integrated density, $\sum_{j=1}^{31} \langle \hat{a}_j^\dagger \hat{a}_j \rangle + \sum_{j=58}^{88} \langle \hat{a}_j^\dagger \hat{a}_j \rangle$) of monomers outside the dimer cluster. (a) Initial states of the cluster are: in the upper black branch, $|-\pi/2\rangle_8^2 | \cdot \rangle_8^2 |\pi/2\rangle_8^2$ (solid line), $|-\pi/2\rangle_8^2 |4_+\rangle_8^2 |\pi/2\rangle_8^2$ (dashed line), and $|-\pi/2\rangle_8^2 |\pi/2\rangle_8^2 |\pi/2\rangle_8^2$ (dot-dashed line); in the lower blue branch, $|\pi\rangle_8^2 | \cdot \rangle_8^2 |0\rangle_8^2$ (solid line), $|\pi\rangle_8^2 |4_+\rangle_8^2 |0\rangle_8^2$ (dashed line), and $|\pi\rangle_8^2 |\pi/2\rangle_8^2 |0\rangle_8^2$ (dot-dashed line). (b) Initial states of the cluster are: $|4_-\rangle_8^2 | \cdot \rangle_8^2 |4_-\rangle_8^2$ (solid line), $|4_-\rangle_8^2 |4_+\rangle_8^2 |4_-\rangle_8^2$ (dashed line), and $|4_-\rangle_8^2 |\pi/2\rangle_8^2 |4_-\rangle_8^2$ (dot-dashed line). The interaction strength is $U = 100J$. Numerical parameters are the same as in Figs. 4 and 5, and the curves terminate when the accumulated cut-off error equals 10^{-2} . The gray lines are obtained from the equivalent effective model, with the time step increased to $1/10J$.

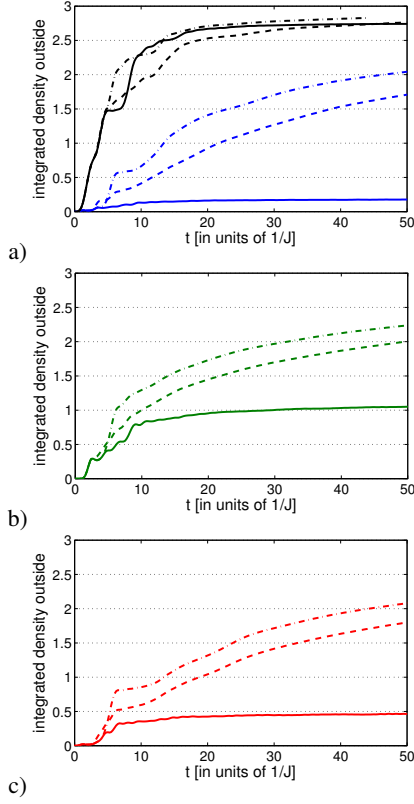


FIG. 7: (Color online) Total population ($\sum_{j=1}^{63} \langle \hat{a}_j^\dagger \hat{a}_j \rangle + \sum_{j=98}^{160} \langle \hat{a}_j^\dagger \hat{a}_j \rangle$) of monomers outside the dimer cluster of 32 sites surrounded by empty lattice, $|\cdot\rangle_{64}^0$, on both sides. (a) Initial states of the cluster are: in the upper black branch, $|\cdot\rangle_{8}^{2-} |\cdot\rangle_{8}^2 |\pi/2\rangle_{8}^{2-} |\cdot\rangle_{8}^{2-}$ (solid line), $|\cdot\rangle_{8}^{2-} |4_+\rangle_{8}^2 |\pi/2\rangle_{8}^{2-} |\cdot\rangle_{8}^{2-}$ (dashed line), and $|\cdot\rangle_{8}^{2-} |\pi/2\rangle_{8}^{2+} |\pi/2\rangle_{8}^{2-} |\cdot\rangle_{8}^{2-}$ (dot-dashed line); in the lower blue branch, $|\pi\rangle_{8}^{2-} |\cdot\rangle_{8}^2 |0\rangle_{8}^{2-} |\pi\rangle_{8}^{2-}$ (solid line), $|\pi\rangle_{8}^{2-} |4_+\rangle_{8}^2 |0\rangle_{8}^{2-} |\pi\rangle_{8}^{2-}$ (dashed line), and $|\pi\rangle_{8}^{2-} |\pi/2\rangle_{8}^{2+} |0\rangle_{8}^{2-} |\pi\rangle_{8}^{2-}$ (dot-dashed line). (b) Initial states of the cluster are: $|4_-\rangle_{8}^2 |\cdot\rangle_{8}^2 |4_-\rangle_{8}^2 |4_-\rangle_{8}^2$ (solid line), $|4_-\rangle_{8}^2 |4_+\rangle_{8}^2 |4_-\rangle_{8}^2 |4_-\rangle_{8}^2$ (dashed line), and $|4_-\rangle_{8}^2 |\pi/2\rangle_{8}^{2+} |4_-\rangle_{8}^2 |4_-\rangle_{8}^2$ (dot-dashed line). (c) Initial states of the cluster are: $|\pi\rangle_{8}^{2-} |\cdot\rangle_{8}^2 |0\rangle_{8}^{2-} |4_-\rangle_{8}^2$ (solid line), $|\pi\rangle_{8}^{2-} |4_+\rangle_{8}^2 |0\rangle_{8}^{2-} |4_-\rangle_{8}^2$ (dashed line), and $|\pi\rangle_{8}^{2-} |\pi/2\rangle_{8}^{2+} |4_-\rangle_{8}^2 |4_-\rangle_{8}^2$ (dot-dashed line). Simulations were performed with the effective model. Bond dimensions $\chi = 300$ are used, and the time step size is $1/10J$. The curves terminate when the accumulated cut-off error equals 10^{-1} .

which we now briefly discuss. The Hamiltonian for the system is

$$\begin{aligned} \hat{H} = & -J_a \sum_j (\hat{a}_j^\dagger \hat{a}_{j+1} + \text{H.a.}) - J_b \sum_j (\hat{b}_j^\dagger \hat{b}_{j+1} + \text{H.a.}) \\ & + \frac{U_a}{2} \sum_j \hat{a}_j^\dagger \hat{a}_j^\dagger \hat{a}_j \hat{a}_j + \frac{U_b}{2} \sum_j \hat{b}_j^\dagger \hat{b}_j^\dagger \hat{b}_j \hat{b}_j \\ & + U_{ab} \sum_j \hat{a}_j^\dagger \hat{a}_j \hat{b}_j^\dagger \hat{b}_j, \end{aligned} \quad (14)$$

where \hat{a}_j (\hat{b}_j) are the bosonic operators for the particles of type a (b) hopping between adjacent sites with the rate J_a

(J_b), while U_a , U_b and U_{ab} are the intra- and inter-species on-site interactions.

Assuming the conditions $U_a, U_b, U_{ab}, |U_a + U_b - 2U_{ab}| \gg J_a, J_b$, we first consider the situation where each lattice site is either empty or contains a single a-b dimer, that is, a pair of strongly interacting (via U_{ab}) particles a and b localized on the same site. Upon adiabatic elimination of the non resonant states containing unpaired particles on neighboring sites [12], we obtain an effective Hamiltonian of the form of Eq. (2), where now the dimer hopping and nearest-neighbor interaction are given by

$$\tilde{J} = -\frac{2J_a J_b}{U_{ab}}, \quad \tilde{B} = -2 \left(\frac{2J_a^2}{U_a} + \frac{2J_b^2}{U_b} + \frac{J_a^2 + J_b^2}{U_{ab}} \right). \quad (15)$$

With all the interactions repulsive, the anisotropy parameter

$$\Delta = \tilde{B}/2\tilde{J} = \frac{J_a}{J_b} \left(\frac{1}{2} + \frac{U_{ab}}{U_a} \right) + \frac{J_b}{J_a} \left(\frac{1}{2} + \frac{U_{ab}}{U_b} \right) \quad (16)$$

is larger than 1 for any finite U_a/U_{ab} or U_b/U_{ab} , and the MI cluster of a-b dimers is stable. But for $U_a/U_{ab}, U_b/U_{ab} \rightarrow \infty$, corresponding to the band insulator for two fermionic species, $\Delta = 1$ and the dimer cluster is unstable.

Inside the $n = n_a + n_b = 2$ ($n_a = n_b = 1$) MI cluster, a hole defect of type a (unpaired particle b) is created by \hat{a}_j , see Fig. 1(e). The defect hops in the cluster with the rate J_a while outside the cluster its hopping rate is J_b . It must be stable and not resonantly converted into a pair of particles b and a single b-hole (unpaired particle a), which requires that $U_b - U_{ab} \gg J_a, J_b$. Neglecting the second-order corrections of the order of $J_{a,b}^2/U_{a,b,ab}$, we have the effective single-particle Hamiltonian (5) with $J_A = J_a$ and $J_B = J_b$. Using the results of Appendix A, we calculate the transmission probability $T(k)$ of the particle through the domain wall separating the regions A and B for various J_b/J_a , which is shown in Fig. 2. At $J_a = J_b$ ($\alpha = 1$) we find an almost perfect transmission for all k , up to a small correction due to finite interactions. The above results equally apply to a hole defect of type b (unpaired particle a) with the replacement $a \leftrightarrow b$.

We have performed numerical simulations of the dynamics of several defects in a dimer cluster surrounded by vacuum using the full model of Eq. (14). For computational reasons, we truncate the local Hilbert space to three bosons of each species per site, which is justified by the facts that, due to the strong interactions, the occupation of a single site by more particles can safely be neglected.

In Fig. 8 we show the behavior of two unpaired particles b, or a-holes, moving in the cluster with different initial velocities. In the case of $J_a = J_b$ (top panel), both defects almost completely leave the cluster upon the first encounter with its walls. For $J_a \neq J_b$, only partial transmission of each defects is recorded, which depends on its initial quasi-momentum, as per Fig. 2. As an example, at $J_a = 2J_b$ (central panel) the unpaired particle b with $k = \pi/2$ can leave the cluster, while that with $k = \pi/4$ can not, as its quasi-momentum is close to the lower band edge.

Fig. 9 illustrates the results for a pair of initially localized defects of different type. Again, for $J_a = J_b$, both defects

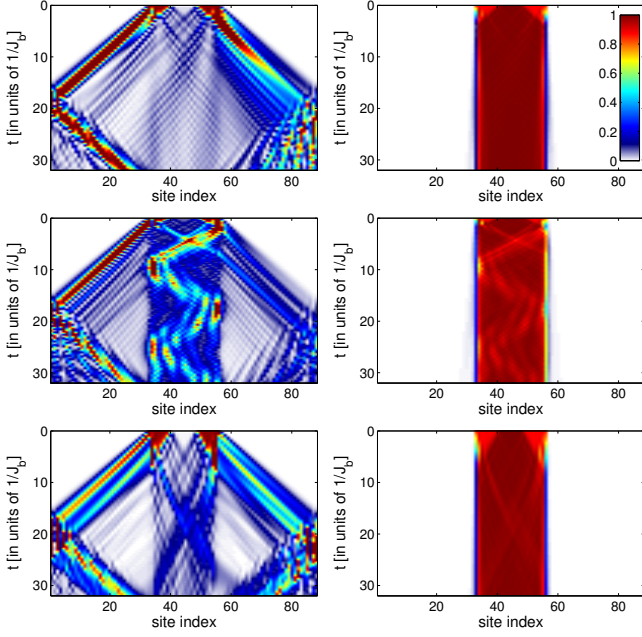


FIG. 8: (Color online) Density of unpaired particles b, or a-holes, in the cluster (left column), and particles a (right column), in the lattice with a MI cluster of a-b dimers spanning 24 sites surrounded by empty lattice, $|\cdot\rangle_{32}^0$, on both sides. The initial state of the cluster $|\cdot\rangle_{32}^0$ corresponds to two a-hole defects moving to the left with velocity $2J_a$, and to the right with velocity $\sqrt{2}J_a$, respectively, while all particles a are dimerized with particles b (no b-hole defects). The parameters are $U_a = U_b = 60J_b$, $U_{ab} = 40J_b$, and $J_a = J_b$ (top panel), $J_a = 2J_b$ (central panel), and $J_a = \frac{1}{2}J_b$ (bottom panel). A TEBD algorithm with bond dimension $\chi = 100$ is used for the time evolution with a fourth order Trotter decomposition and time step size $1/50J_b$, with the particle number conservation for each species explicitly included in the MPS.

easily leave the cluster through its walls, but when $J_a \neq J_b$, only a fraction of the population of each defect leaves the cluster after the first collision with its wall. Note, however, that since the two types of hole defects have different effective mass, their collisions with each other and the walls of the cluster can effectively redistribute their quasi-momenta, and no trimer defects are required to purify the MI cluster.

VII. SUMMARY

To conclude, in one-dimensional MI clusters of repulsively-bound dimers of bosons [9], hole defects (unpaired particles, or monomers) can evaporate through the cluster boundaries, taking away the entropy of the system. In the case of dimers of identical bosons, only part of the monomer population can leave the cluster unassisted. Complete evaporation of the hole defects is possible in the presence of catalyzing particle defects (trimers), which efficiently thermalize the hole defects via the quasi-momentum redistributing collisions. The particle defects themselves can not leave the cluster, due to the large energy mismatch $2U$ between a single excess particle

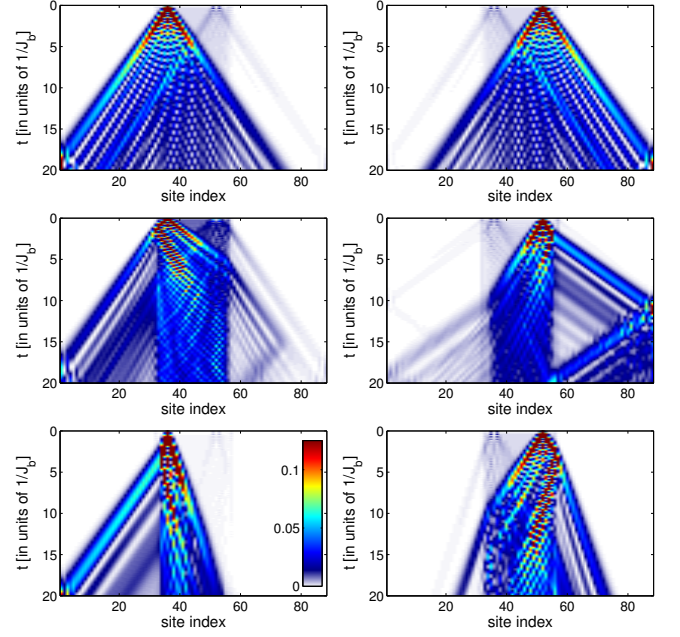


FIG. 9: (Color online) Dynamics of an initially localized unpaired particle b, or a-hole, in the cluster (left column), and an unpaired particle a, b-hole, in the cluster (right column), for the initial cluster state $|4_{-a}\rangle_8^2|\cdot\rangle_8^2|4_{-b}\rangle_8^2$. All parameters are as in Fig. 8, and the bond dimension of the TEBD is $\chi = 200$.

on top of the $n = 2$ MI cluster and on an empty lattice.

In the case of dimers composed of two different bosonic species, the defect evaporation proceeds by itself, without the need of any catalyzing species.

The system studied in this paper is amenable to experimental investigations with cold atoms in optical lattices [3]. To prepare the cluster of dimers surrounded by lattice vacuum, one starts with an optical lattice superimposed by a shallow confining potential populated by the MI phases with occupation numbers of $n = 0, 1, 2$ in successive spatial shells [20, 21], followed by removal of all the atoms outside the central $n = 2$ MI region [22]. The homogeneous lattice potential is then achieved by turning off the shallow confining potential, while the spatial distribution of the defects and their dynamics inside and outside the dimer cluster can be resolved using non-destructive single-site addressing techniques [23–25].

Acknowledgments

D. M. and M. F. acknowledge financial support through the SFB/TR49 of the Deutsche Forschungsgemeinschaft. D. P. acknowledges the support of the Humboldt Foundation.

Appendix A: Transmission of a particle through a domain wall

Here we calculate the probability of transmission of a particle with quasi-momentum k through a domain wall, as per Eq. (5). For the particle incident from the left, we solve the

stationary Schrödinger equation using the standard scattering ansatz for the wave function,

$$\psi_j = \begin{cases} e^{ikj} + \rho e^{-ikj} & j \leq 0 \\ \tau e^{ik'j} & j \geq 0 \end{cases}, \quad (\text{A1})$$

where ρ and τ are the complex reflection and transmission amplitudes. The energy eigenvalue is $E_k = E_k^{(\text{A})} = -2J_A \cos(k) = -2J_B \cos(k') = E_{k'}^{(\text{B})}$, and therefore the reflection is given by

$$k' = \cos^{-1} \left(\frac{\cos(k)}{\alpha} \right). \quad (\text{A2})$$

Thus the transmission vanishes if $\cos(k) \geq \alpha$, where $\alpha = J_B/J_A$. (In this paper we are primarily concerned with the case of $\alpha = 1/2$, except for Sec. VI.)

Continuity at $j = 0$ implies $1 + \rho = \tau$, which together with the Schrödinger equation at $j = 0$,

$$(\hat{H}\psi)_0 = -J_A\psi_{-1} - J_B\psi_1 = E_k\psi_0, \quad (\text{A3})$$

yields

$$\rho = \frac{J_B e^{ik'} + J_A e^{-ik} - 2J_A \cos(k)}{-J_B e^{ik'} - J_A e^{ik} + 2J_A \cos(k)}. \quad (\text{A4})$$

The current density in the two parts of the system is given by

$$f_j = \begin{cases} f_j^{(\text{A})} = -iJ_A(\psi_j^* \psi_{j+1} - \psi_j \psi_{j+1}^*) & j < 0 \\ f_j^{(\text{B})} = -iJ_B(\psi_j^* \psi_{j+1} - \psi_j \psi_{j+1}^*) & j \geq 0 \end{cases}. \quad (\text{A5})$$

One can readily verify that

$$\frac{d}{dt} \psi_j^* \psi_j = (-i\hat{H}\psi)_j^* \psi_j + \psi_j^* (-i\hat{H}\psi)_j = -(f_j - f_{j-1}). \quad (\text{A6})$$

For the state of Eq. (A1), we have

$$f_{\text{in}} = 2J_A \sin(k), \quad (\text{A7a})$$

$$f_{\text{ref}} = -2J_A \sin(k) \rho^* \rho, \quad (\text{A7b})$$

$$f_{\text{trans}} = 2J_B \sin(k') \tau^* \tau, \quad (\text{A7c})$$

so that the reflection and transmission probabilities are

$$R = \left| \frac{f_{\text{ref}}}{f_{\text{in}}} \right| = \rho^* \rho, \quad (\text{A8})$$

$$T = \left| \frac{f_{\text{trans}}}{f_{\text{in}}} \right| = \alpha \frac{\sin(k')}{\sin(k)} \tau^* \tau. \quad (\text{A9})$$

One can verify that $T + R = 1$ as it should.

Appendix B: Two particle Hamiltonian in quasi-momentum space

We consider a pair of distinguishable, locally interacting particles on a lattice described by Hamiltonian

$$\begin{aligned} \hat{H} = & -J_a \left(\sum_{j=1}^{L-1} \hat{a}_j^\dagger \hat{a}_{j+1} + \gamma \hat{a}_L^\dagger \hat{a}_1 + \text{H.a.} \right) \\ & -J_t \left(\sum_{j=1}^{L-1} \hat{t}_j^\dagger \hat{t}_{j+1} + \gamma \hat{t}_L^\dagger \hat{t}_1 + \text{H.a.} \right) \\ & + U \sum_{j=1}^L \hat{a}_j^\dagger \hat{a}_j \hat{t}_j^\dagger \hat{t}_j, \end{aligned} \quad (\text{B1})$$

where the periodic and open boundary conditions correspond, respectively, to $\gamma = 1$ and $\gamma = 0$. The operators \hat{a}_j^\dagger and \hat{t}_j^\dagger create soft-core particles interacting via U , which is convenient for the exact numerical simulations presented in Sec. IV B.

In quasi-momentum representation, $k = 2\pi\nu/L$ ($\nu = \lfloor -\frac{L}{2} + 1 \rfloor \dots \lfloor \frac{L}{2} \rfloor$), we have $\hat{a}_k^\dagger = \frac{1}{\sqrt{L}} \sum_{j=1}^L e^{ikj} \hat{a}_j^\dagger$ and $\hat{t}_k^\dagger = \frac{1}{\sqrt{L}} \sum_{j=1}^L e^{ikj} \hat{t}_j^\dagger$ and two such particles have a probability L^{-1} to be on the same real lattice site. The Hamiltonian then reads

$$\begin{aligned} \hat{H} = & -2J_a \sum_k \cos(k) \hat{a}_k^\dagger \hat{a}_k + \frac{(1-\gamma)J_a}{L} \sum_{k,k'} \hat{a}_k^\dagger \hat{a}_{k'} (e^{ik} + e^{-ik'}) \\ & -2J_t \sum_k \cos(k) \hat{t}_k^\dagger \hat{t}_k + \frac{(1-\gamma)J_t}{L} \sum_{k,k'} \hat{t}_k^\dagger \hat{t}_{k'} (e^{ik} + e^{-ik'}) \\ & + \frac{U}{L} \sum_{k,k',k''} \hat{a}_k^\dagger \hat{a}_{k'} \hat{t}_{k''}^\dagger \hat{t}_{(k+k''-k')}. \end{aligned} \quad (\text{B2})$$

Appendix C: Effective theory for monomers and trimers

The non-locality of the effective theory presented in Sec. V A might seem surprising at first sight. From the point of view of quantum information theory, however, the Hamiltonian (9) is still local, in the sense that the commutator $[\tilde{H}_j, \tilde{H}_{j'}]$ vanishes except for $j' = j \pm 1$, despite the fact that the support of any two $\tilde{H}_j, \tilde{H}_{j'}$ has a large overlap. This property should always be conserved in any effective theory, since it guarantees that correlations in the model system travel with the same maximal velocity as in the full system [26, 27]. This property also permits the application of the TEBD numerical method, in conjunction with the conservation of the total particle number, to the effective model. For then all the basis states used in the TEBD (eigenstates of the reduced density matrices for all bi-partitions of the lattice) are, by construction, the eigenstates of the total particle number in the corresponding subsystem. Since the total particle number is the only observable that enters Hamiltonian (9) via $\hat{P}_j^{n_r}$, this

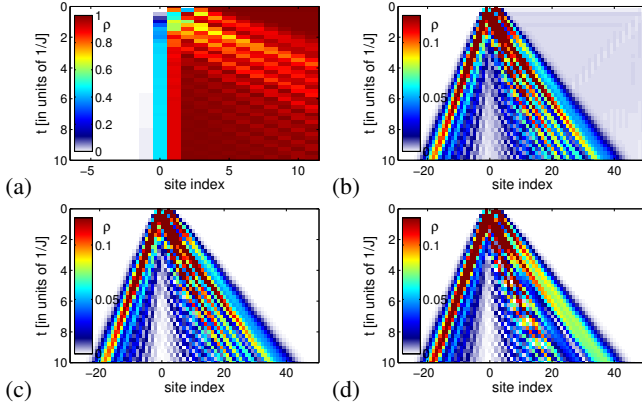


FIG. 10: (Color online) Comparison of the full Bose-Hubbard dynamics, Eq. (1) with $U = 100J$, (a) and (b), with the effective model, Eq. (9), (c). The initial state contains a MI cluster of dimers on sites $j \geq 1$ and localized monomers at sites $j = -1$ and $j = 2$. The density of dimers is shown in (a), and the density of monomers in (b)-(d). Note that the cluster boundary is shifted upon particle crossing, which manifests in (a) as a smoothing of step in the dimer density. The effective Hamiltonian without moving boundaries, $\hat{H} = \sum_{j=1}^{L-1} \hat{H}_j^{(\Theta(j))}$, yields the dynamics of (d).

type of non-locality does not introduce additional difficulties in the use of the TEBD method.

The effective model can also be extended to higher orders in perturbation theory. In second order, this introduces nearest neighbor interactions, local potentials and effective exchange between monomers and trimers. All these terms are of the order of J^2/U and depend on Θ , which can now assume four different values depending on the type of bond between sites j and $j + 1$. Another term of the same order describes hole defect hopping to the next-nearest neighbor site in the cluster. As this is spanning three sites, it also depends on the state of the central site and requires more values of Θ . The presence of such a longer-range term would necessitate a more general numerical simulation algorithm than TEBD. We have verified, however, that the effective Hamiltonian (10) containing only the terms first order in J already captures all the essential physics discussed in this paper.

In Fig. 10 we compare the dynamics of hole defects obtained from the full and effective models, which agree very well for large interaction strength $U \gg J$. Observe, however, that a local theory neglecting the motion of the cluster boundaries, Fig. 10(d), and therefore violating the conservation of the total number of dimers and bare particles, does not describe the dynamics quantitatively correctly.

Appendix D: MPS representation of the initial state

Here we show how to construct an exact MPS representation for a lattice containing fixed number of bosons each in a certain single particle eigenstate. The resulting MPS will be in the canonical representation [28] and symmetric [29], i.e., it will be an eigenstate of the total particle number by construction. The construction is analogous to that of matrix product

operators for fixed total particle number [30].

The single particle state is given by a normalized wavefunction ϕ_j . In the examples of Sec. VB, we have $\phi_j = \frac{1}{\sqrt{L}} e^{ikj}$ with fixed quasi-momentum k . The corresponding state $|\Psi^1\rangle = \sum_{j=1}^L \phi_j \hat{a}_j^\dagger |0\rangle$ can be written as

$$|\Psi^1\rangle = (\sqrt{q_m} \hat{a}_A^\dagger + \sqrt{1 - q_m} \hat{a}_B^\dagger) |0\rangle_A \otimes |0\rangle_B, \quad (D1)$$

where sub-lattice A spans sites 1 to m and sub-lattice B is from $m + 1$ to L , while $q_m = \sum_{j=1}^m \phi_j^* \phi_j$ is the single particle probability of being in A. The bosonic creation operators \hat{a}_A^\dagger and \hat{a}_B^\dagger are defined by

$$\hat{a}_A^\dagger = \frac{1}{\sqrt{q_m}} \sum_{j=1}^m \phi_j \hat{a}_j^\dagger, \quad \hat{a}_B^\dagger = \frac{1}{\sqrt{1 - q_m}} \sum_{j=m+1}^L \phi_j \hat{a}_j^\dagger. \quad (D2)$$

The state of the lattice with N particles in the same single particle state can then be expressed as

$$\begin{aligned} |\Psi^N\rangle &= \frac{1}{\sqrt{N!}} (\sqrt{q_m} \hat{a}_A^\dagger + \sqrt{1 - q_m} \hat{a}_B^\dagger)^N |0\rangle_A \otimes |0\rangle_B \\ &= \frac{1}{\sqrt{N!}} \sum_{l=0}^N \binom{N}{l} \\ &\quad \times (\sqrt{q_m} \hat{a}_A^\dagger)^l (\sqrt{1 - q_m} \hat{a}_B^\dagger)^{N-l} |0\rangle_A \otimes |0\rangle_B, \end{aligned} \quad (D3)$$

and the density matrix of the system is

$$\begin{aligned} |\Psi^N\rangle \langle \Psi^N| &= \frac{1}{N!} \sum_{l, l'=0}^N \binom{N}{l} \binom{N}{l'} \\ &\quad \times (\sqrt{q_m} \hat{a}_A^\dagger)^l |0\rangle_A \langle 0|_A (\sqrt{q_m} \hat{a}_A)^{l'} \\ &\quad \otimes (\sqrt{1 - q_m} \hat{a}_B^\dagger)^{N-l} |0\rangle_B \langle 0|_B (\sqrt{1 - q_m} \hat{a}_B)^{N-l'} \end{aligned} \quad (D4)$$

The density matrix of subsystem A is

$$\begin{aligned} \rho_A &= \text{Tr}_B [|\Psi^N\rangle \langle \Psi^N|] \\ &= \frac{1}{N!} \sum_{l=0}^N \binom{N}{l}^2 (N-l)! (1 - q_m)^{N-l} \\ &\quad \times (\sqrt{q_m} \hat{a}_A^\dagger)^l |0\rangle_A \langle 0|_A (\sqrt{q_m} \hat{a}_A)^l. \end{aligned} \quad (D5)$$

Note that ρ_A has at most $\chi = N + 1$ nonzero eigenvalues, one for each possible distribution of the N particles between A and B. With $\hat{P}_l^{[A]}$ the projector onto the l particle sector of subsystem A, the probability of finding l particles in A is

$$\begin{aligned} \text{Tr}_A [\rho_A \hat{P}_l^{[A]}] &= \frac{1}{N!} \sum_{l=0}^N \binom{N}{l}^2 (N-l)! l! (1 - q_m)^{N-l} (q_m)^l \\ &= \sum_{l=0}^N \binom{N}{l} (1 - q_m)^{N-l} (q_m)^l \\ &= B_{q_m}(l|N), \end{aligned} \quad (D6)$$

which is a binomial distribution.

We can now construct $|\Psi^N\rangle$ as a matrix product state in the canonical [28] form. Given a bi-partition of the lattice, its Schmidt decomposition is

$$|\Psi^N\rangle = \sum_{l=0}^N \lambda_l^{[m]} |\Psi^l\rangle_A \otimes |\Psi^{N-l}\rangle_B, \quad (\text{D7})$$

with $|\Psi^l\rangle_A = \frac{1}{\sqrt{l!}} (\hat{a}_A^\dagger)^l |0\rangle_A$ and $|\Psi^{N-l}\rangle_B = \frac{1}{\sqrt{(N-l)!}} (\hat{a}_B^\dagger)^{(N-l)} |0\rangle_B$. The MPS will have bond dimension of $\chi = N + 1$. The probability of finding l particles to the left of bond m is

$$(\lambda_l^{[m]})^2 = B_{q_m}(l|N). \quad (\text{D8})$$

We then continue with the Schmidt decomposition at the following bond. The remaining task is to determine the coefficients of

$$|\Psi^N\rangle = \sum_{l=0}^N \sum_{r=l}^N \lambda_l^{[m]} \Gamma_{lr}^{[m+1]} \lambda_r^{[m+1]} \times |\Psi^l\rangle_A \otimes |\Psi^{r-l}\rangle_{m+1} \otimes |\Psi^{N-r}\rangle_{B'}. \quad (\text{D9})$$

The λ tensors are already known from (D8). The sub-chain B' comprises sites $m+2$ to L . Thus $(\lambda_l^{[m]})^2 |\Gamma_{lr}^{[m+1]}|^2 (\lambda_r^{[m+1]})^2$ is the probability of finding $N-r$ particles on the right of bond $m+1$ and l particles on the left of bond m , resulting in

$$\begin{aligned} |\Gamma_{lr}^{[m+1]}|^2 &= \frac{B_{\frac{q_m}{q_{m+1}}}(l|r)}{B_{q_m}(l|N)} \\ &= \frac{r!(N-l)!}{(r-l)!N!} q_{m+1}^{-r} (q_{m+1} - q_m)^{r-l} (1 - q_m)^{l-N}. \end{aligned} \quad (\text{D10})$$

For the phase to be correct, we obviously have to set

$$\arg(\Gamma_{lr}^{[m+1]}) = (r-l) \arg(\phi_{m+1}). \quad (\text{D11})$$

Equations (D8), (D10), and (D11) completely determine the tensors Γ and λ . Note that in this particular case, the value of the bond index of $\lambda^{[m]}$ has a physical meaning of the number of particles to the left of bond m . The resulting MPS is an eigenstate of the total particle number, which can be used in TEBD implementations that take advantage of particle number conservation explicitly, as in this paper.

The construction is more complicated when one intends to prepare N_α particles in different single particle states $\alpha = 1, 2, \dots, M$. From simple combinatorial considerations, we deduce that the Schmidt rank will be $\chi = \prod_\alpha (1 + N_\alpha)$, i.e., exponentially large in the number M of different single particle states. (This implies that, as a starting point for dynamical simulations, one can construct an exact MPS for the ground state of non-interacting bosons, as done in [31], but not for non-interacting fermions.) The exact expression in terms of the $q_{m,\alpha}$ will contain overlaps between the different single particle states, which in general are finite in any subsystem even if the single particle states are orthogonal on the entire lattice.

-
- [1] N. W. Ashcroft and N. D. Mermin. *Solid state physics*. Holt, Rinehart and Winston, 1976.
 - [2] A. L. Fetter and J. D. Walecka. *Quantum theory of many particle systems*. McGraw-Hill, 1971.
 - [3] I. Bloch, J. Dalibard, and W. Zwerger. Many-body physics with ultracold gases. *Rev. Mod. Phys.*, 80(3):885, July 2008.
 - [4] M. Lewenstein, A. Sanpera, V. Ahufinger, B. Damski, A. Sen(De), and U. Sen. Ultracold atomic gases in optical lattices: mimicking condensed matter physics and beyond. *Adv. Phys.*, 56(2):243–379, May 2007.
 - [5] M. P. A. Fisher, P. B. Weichman, G. Grinstein, and D. S. Fisher. Boson localization and the superfluid-insulator transition. *Phys. Rev. B*, 40(1):546–570, July 1989.
 - [6] K. Winkler, G. Thalhammer, F. Lang, R. Grimm, J. Hecker Denschlag, A. J. Daley, A. Kantian, H. P. Büchler, and P. Zoller. Repulsively bound atom pairs in an optical lattice. *Nature*, 441(7095):853–856, June 2006.
 - [7] R. Piil and K. Molmer. Tunneling couplings in discrete lattices, single-particle band structure, and eigenstates of interacting atom pairs. *Phys. Rev. A*, 76(2):023607, August 2007.
 - [8] M. Valiente and D. Petrosyan. Two-particle states in the hubbard model. *J. Phys. B: At., Mol. Opt. Phys.*, 41(16):161002, August 2008.
 - [9] D. Petrosyan, B. Schmidt, J. R. Anglin, and M. Fleischhauer. Quantum liquid of repulsively bound pairs of particles in a lattice. *Phys. Rev. A*, 76(3):033606, September 2007.
 - [10] M. Valiente, D. Petrosyan, and A. Saenz. Three-body bound states in a lattice. *Phys. Rev. A*, 81(1):011601(R), January 2010.
 - [11] F. Heidrich-Meisner, S. R. Manmana, M. Rigol, A. Muramatsu, A. E. Feiguin, and E. Dagotto. Quantum distillation: Dynamical generation of low-entropy states of strongly correlated fermions in an optical lattice. *Phys. Rev. A*, 80(4):041603(R), October 2009.
 - [12] B. Schmidt, M. Bortz, S. Eggert, M. Fleischhauer, and D. Petrosyan. Attractively bound pairs of atoms in the bose-hubbard model and antiferromagnetism. *Phys. Rev. A*, 79(6):063634, June 2009.
 - [13] D. Muth, M. Fleischhauer, and B. Schmidt. Discretized versus continuous models of p -wave interacting fermions in one dimension. *Phys. Rev. A*, 82(1):013602, July 2010.
 - [14] M. Valiente and D. Petrosyan. Scattering resonances and two-particle bound states of the extended hubbard model. *J. Phys. B: At., Mol. Opt. Phys.*, 42(12):121001, June 2009.
 - [15] M. Valiente. Lattice two-body problem with arbitrary finite-

- range interactions *arXiv preprint e-1668-2011*. *Phys. Rev. A*, 81(4):042102, April 2010.
- [16] A. J. Daley, C. Kollath, U. Schollwöck, and G. Vidal. Time-dependent density-matrix renormalization-group using adaptive effective hilbert spaces. *J. Stat. Mech.*, page P04005, April 2004.
 - [17] S. R. White and A. E. Feiguin. Real-time evolution using the density matrix renormalization group. *Phys. Rev. Lett.*, 93(7):076401, August 2004.
 - [18] G. Vidal. Efficient classical simulation of slightly entangled quantum computations. *Phys. Rev. Lett.*, 91(14):147902, October 2003.
 - [19] A. J. Daley, S. R. Clark, D. Jaksch, and P. Zoller. Numerical analysis of coherent many-body currents in a single atom transistor. *Phys. Rev. A*, 72(4):043618, October 2005.
 - [20] G. K. Campbell, J. Mun, M. Boyd, P. Medley, A. E. Leanhardt, L. G. Marcassa, D. E. Pritchard, and W. Ketterle. Imaging the mott insulator shells by using atomic clock shifts. *Science*, 313(5787):649–652, August 2006.
 - [21] S. Fölling, A. Widera, T. Müller, F. Gerbier, and I. Bloch. Formation of spatial shell structure in the superfluid to mott insulator transition. *Phys. Rev. Lett.*, 97(6):060403, August 2006.
 - [22] P. Würtz, T. Langen, T. Gericke, A. Koglbauer, and H. Ott. Experimental demonstration of single-site addressability in a two-dimensional optical lattice. *Phys. Rev. Lett.*, 103(8):080404, August 2009.
 - [23] W. S. Bakr, J. I. Gillen, A. Peng, S. Fölling, and M. Greiner. A quantum gas microscope for detecting single atoms in a hubbard-regime optical lattice. *Nature*, 462(7269):74–U80, November 2009.
 - [24] W. S. Bakr, A. Peng, M. E. Tai, R. Ma, J. Simon, J. I. Gillen, S. Fölling, L. Pollet, and M. Greiner. Probing the superfluid-to-mott insulator transition at the single-atom level. *Science*, 329(5991):547–550, July 2010.
 - [25] J. F. Sherson, C. Weitenberg, M. Endres, M. Cheneau, I. Bloch, and S. Kuhr. Single-atom-resolved fluorescence imaging of an atomic mott insulator. *Nature*, 467(7311):68–U97, September 2010.
 - [26] S. Bravyi, M. B. Hastings, and F. Verstraete. Lieb-robinson bounds and the generation of correlations and topological quantum order. *Phys. Rev. Lett.*, 97(5):050401, August 2006.
 - [27] J. Eisert and T. J. Osborne. General entanglement scaling laws from time evolution. *Phys. Rev. Lett.*, 97(15):150404, October 2006.
 - [28] D. Perez-Garcia, F. Verstraete, M. M. Wolf, and J. I. Cirac. Matrix product state representations. *Quant. Inf. Comp.*, 7(5-6):401–430, July 2007.
 - [29] U. Schollwöck. The density-matrix renormalization group in the age of matrix product states. *Ann. Phys. (New York)*, 326(1):96–192, January 2011.
 - [30] D. Muth. Particle number conservation in quantum many-body simulations with matrix product operators. *J. Stat. Mech.*, page P11020, April 2011.
 - [31] D. Muth, B. Schmidt, and M. Fleischhauer. Fermionization dynamics of a strongly interacting one-dimensional bose gas after an interaction quench. *New J. Phys.*, 12:083065, August 2010.